



Am J Physiol Renal Physiol. 2015 Oct 15; 309(8): F708–F719.

PMCID: PMC4609917

Published online 2015 Jul 15.

PMID: [26180238](#)

doi: 10.1152/ajprenal.00187.2015; 10.1152/ajprenal.00187.2015

Predicted effects of nitric oxide and superoxide on the vasoactivity of the afferent arteriole

[Anita T. Layton](#)¹ and [Aurélie Edwards](#)^{✉2}

¹Department of Mathematics, Duke University, Durham, North Carolina; and

²Sorbonne Universités, UPMC Université Paris 06, Université Paris Descartes, Sorbonne Paris Cité, INSERM UMRS 1138, CNRS ERL 8228, Centre de Recherche des Cordeliers, Paris, France

[✉]Corresponding author.

Address for reprint requests and other correspondence: A. Edwards, Centre de Recherche des Cordeliers, 15 rue de l'Ecole de Médecine, 75006 Paris, France (e-mail: aurelie.edwards@crc.jussieu.fr).

Received 2015 May 1; Accepted 2015 Jul 9.

Copyright © 2015 the American Physiological Society

Abstract

We expanded a published mathematical model of an afferent arteriole smooth muscle cell in rat kidney (Edwards A, Layton, AT. *Am J Physiol Renal Physiol* 306: F34–F48, 2014) to understand how nitric oxide (NO) and superoxide (O_2^-) modulate the arteriolar diameter and its myogenic response. The present model includes the kinetics of NO and O_2^- formation, diffusion, and reaction. Also included are the effects of NO and its second messenger cGMP on cellular Ca^{2+} uptake and efflux, Ca^{2+} -activated K^+ currents, and myosin light chain phosphatase activity. The model considers as well pressure-induced increases in O_2^- production, O_2^- -mediated regulation of L-type Ca^{2+} channel conductance, and increased O_2^- production in spontaneous hypertensive rats (SHR). Our results indicate that elevated O_2^- production in SHR is sufficient to account for observed differences between normotensive and hypertensive rats in the response of the afferent arteriole to NO synthase inhibition, Tempol, and angiotensin II at baseline perfusion pressures. In vitro, whether the myogenic response is stronger in SHR remains uncertain. Our model predicts that if mechanosensitive cation channels are not modulated by O_2^- , then fractional changes in diameter induced by pressure elevations should be smaller in SHR than in normotensive rats. Our results also suggest that most NO diffuses out of the smooth muscle cell without being consumed, whereas most O_2^- is scavenged, by NO and superoxide dismutase. Moreover, the predicted effects of superoxide on arteriolar constriction are not predominantly due to its scavenging of NO.

Keywords: afferent arteriole, myogenic response, nitric oxide, reactive oxygen species, mathematical model

TO MAINTAIN NORMAL KIDNEY function, renal blood flow is tightly regulated over a wide range of perfusion pressure values (7, 33). The two major renal autoregulatory mechanisms are the myogenic response and the tubuloglomerular feedback. The myogenic response elicits a reflex constriction in the preglomerular vasculature in response to a rise in intravascular pressure, thereby generating a compensatory increase in vascular resistance to stabilize the glomerular filtration rate (GFR). The tubuloglomerular feedback mechanism balances GFR with tubular reabsorptive capacity (7, 23, 33). The myogenic response and tubuloglomerular feedback share a common effector in the afferent arteriole.

Nitric oxide (NO) functions as a vasodilator and is an important factor in the maintenance of blood pressure and renal perfusion. Chronic inhibition of NO synthase (NOS) reduces medullary blood flow (6) and, owing to the inhibitory effects of NO on thick ascending limb salt transport, is associated with sodium retention and the development of hypertension (43). NO induces vasodilation through a complex web of signaling pathways; thus a goal of this study is to develop a detailed model of the afferent arteriole smooth muscle cell that incorporates the effects of NO and to use that model to assess the relative contribution of individual effects.

In contrast, superoxide (O_2^-) acts to reduce medullary blood flow (14) and enhance thick ascending limb sodium reabsorption (19). Elevated production of O_2^- has been shown to contribute significantly to the functional alterations of arteries in hypertension (2, 22). Thus the balance between NO and O_2^- likely plays a key role in the long-term control of blood pressure. Indeed, enhanced scavenging of NO by O_2^- , and hence the removal of its buffering influence on vasoconstrictor systems, are believed to contribute significantly to the development of endothelial dysfunction and hypertension (57).

The spontaneously hypertensive rat (SHR) is a widely used animal model of essential hypertension. One interesting characteristic of the SHR is that its autoregulatory plateau (i.e., the range of renal perfusion pressures where single nephron GFR remains approximately constant) is shifted to the right to coincide with its elevated blood pressure range (30). As a result, glomerular capillaries in SHR are better protected against barotrauma, and SHR are substantially less susceptible to renal injury than other models of hypertension (44). The right-shift of the SHR autoregulatory curve has been attributed to the enhanced vasoconstriction exhibited by their afferent arterioles in response to increased perfusion pressure, compared with Wistar-Kyoto (WKY) rats (29).

Studies in SHR indicate that the development of hypertension is associated with increased production of O_2^- in vascular tissues (59, 64). Ren et al. (46) demonstrated in microdissected afferent arterioles that elevated transmural pressure increases O_2^- production, and this increase is particularly pronounced in SHR. These investigators postulated that the enhanced myogenic response of SHR can be attributed, in part, to the activation of NADPH oxidase (NOX) and the increased generation of O_2^- . The principal goal of this study is to use a detailed mathematical model of the afferent arteriole smooth muscle cell to investigate how altering the balance between NO and O_2^- affects arteriolar vasoconstriction.

MATHEMATICAL MODEL

We expanded a published model of an afferent arteriole smooth muscle cell in rat kidney (11) to include the effects of NO and O_2^- . Figure 1 displays the main signaling pathways for which our model accounts. The contractile force exerted on the cell depends on the fraction of myosin light chains (MLC) that is phosphorylated. The model represents the effects of NO and O_2^- on plasma membrane (PMCA) and sarco/endoplasmic reticulum (SERCA) Ca^{2+} pumps, Na^+K^+ -ATPase, Ca^{2+} -gated K^+ channels, and L-type Ca^{2+} channels and on the activation of myosin light chain phosphatase (MLCP).

Ion and Charge Conservation Equations

The cytosolic concentrations of K^+ , Na^+ , Cl^- , and Ca^{2+} as a function of time are determined by considering the sum of their respective fluxes into the cytosol and integrating the following differential equations:

$$\frac{d[K]_{\text{cyt}}}{dt} = - \frac{(I_{K,b} + I_{K,ir} + I_{K,v} + I_{K,Ca} - 2I_{NaK})}{F \cdot \text{vol}_{\text{cyt}}} \quad (1)$$

$$\frac{d[Na]_{\text{cyt}}}{dt} = - \frac{(I_{Na,b} + I_{Na,Pres} + 3I_{NaK} + 3I_{NCX})}{F \cdot \text{vol}_{\text{cyt}}} + \frac{J_{NaCl}}{\text{vol}_{\text{cyt}}} \quad (2)$$

$$\frac{d[Cl]_{\text{cyt}}}{dt} = + \frac{(I_{Cl,b} + I_{Cl,Ca})}{F \cdot \text{vol}_{\text{cyt}}} + \frac{J_{NaCl}}{\text{vol}_{\text{cyt}}} \quad (3)$$

$$\frac{d[Ca]_{\text{cyt}}}{dt} = - \frac{(I_{Ca,b} + I_{Ca,Pres} + I_{PMCA} + I_{Ca,L} - 2I_{NCX} + I_{SERCA} - I_{RyR} - I_{IP3R})}{2F \cdot \text{vol}_{\text{cyt,Ca}}} + (R_{CaM}^{\text{cyt}} + R_{Bf}^{\text{cyt}}) \quad (4)$$

where F is Faraday's constant and vol_{cyt} and $\text{vol}_{\text{cyt,Ca}}$ denote the total volume of the cytosol and the volume that is available to Ca^{2+} , respectively. The convention adopted in this study is that exit of positive charge from the cell is a positive current. Conversely, exit of negative charge is a negative current. The following currents are not affected by NO and O_2^- and can be found in Ref. 11: the background current of ion i ($I_{i,b}$), potassium currents across inward-rectifier and delayed-rectifier channels ($I_{K,ir}$ and $I_{K,v}$), the current across Na^+/Ca^{2+} exchangers (I_{NCX}), the flux across NaCl cotransporters (J_{NaCl}), the chloride current across Ca^{2+} -activated Cl^- channels ($I_{Cl,Ca}$), as well as calcium currents mediated by ryanodine and inositol-trisphosphate receptors (I_{RyR} and I_{IP3R}). Other currents are described below. Calcium buffering by calmodulin (R_{CaM}^{cyt}) and by other cytosolic buffers (R_{Bf}^{cyt}) is described in Ref. 11.

In the sarcoplasmic reticulum (SR), we have:

$$\frac{d[\text{Ca}]_{\text{SR}}}{dt} = + \frac{(I_{\text{SERCA}} - I_{\text{RyR}} - I_{\text{IP3R}})}{2F \cdot \text{vol}_{\text{SR}}} + R_{\text{Calseq}}^{\text{SR}} \quad (5)$$

where vol_{SR} denotes the volume of the SR. The reaction term $R_{\text{Calseq}}^{\text{SR}}$ accounts for the buffering of Ca^{2+} by calsequestrin and is described in Ref. [11](#).

The transmembrane potential V_m is determined by the net sum of the currents flowing across the plasma membrane ([11](#)).

Kinetics of Formation of NO and O_2^-

Nitric oxide. The kinetics of NO and O_2^- formation, diffusion, and reaction are modeled as in our previous study of NO-induced vasodilation of descending vasa recta ([10](#)). We assume that the only source of NO is the endothelium. Once generated, endothelial NO diffuses into the smooth muscle cell where it is partly consumed by several scavengers (e.g., O_2^- , O_2 , and thiols) while the rest diffuses across the abluminal cell membrane into the interstitium. Conservation of NO is given by:

$$\text{vol}_{\text{cyt}} \frac{d[\text{NO}]_{\text{cyt}}}{dt} = \frac{A}{2} J_{\text{NO}}^{\text{endo}} - \frac{A}{2} P_{\text{NO}} [\text{NO}]_{\text{cyt}} - \text{vol}_{\text{cyt}} k_{\text{NO}, \text{O}_2^-} [\text{NO}]_{\text{cyt}} [\text{O}_2^-]_{\text{cyt}} - \text{vol}_{\text{cyt}} k_{\text{NO}, \text{cons}} [\text{NO}]_{\text{cyt}} \quad (6)$$

where A (taken as $5.5 \times 10^{-6} \text{ cm}^2$) is the total membrane surface area; $J_{\text{NO}}^{\text{endo}}$, which denotes the NO flux from the endothelium, is fixed at $6.4 \times 10^{-6} \mu\text{mol} \cdot \text{cm}^{-2} \cdot \text{s}^{-1}$ so that the basal concentration of NO is on the order of 100 nM, as measured in tubular fluid in vivo ([36](#)). The second term on the right-hand side represents NO diffusion towards the interstitium: P_{NO} (estimated as 0.03 cm/s) is the cell membrane permeability to NO, and peritubular $[\text{NO}]$ is assumed to be much smaller than $[\text{NO}]_{\text{cyt}}$. The third term describes the reaction between NO and O_2^- that yields peroxynitrite (ONOO^-):



where the rate constant $k_{\text{NO}, \text{O}_2^-}$ is set to $6.7 \times 10^3 \mu\text{M}^{-1} \cdot \text{s}^{-1}$ ([25](#)). Scavenging of NO by species other than O_2^- is lumped into a first-order process with a rate constant denoted by $k_{\text{NO}, \text{cons}}$, taken as 0.01 s^{-1} .

Superoxide. Whereas NO is produced by the endothelium, O_2^- is generated within the smooth muscle cell. It then either exits the cell via diffusion or reacts with scavengers. Changes in cytosolic $[\text{O}_2^-]$ are given by:

$$\text{vol}_{\text{cyt}} \frac{d[\text{O}_2^-]_{\text{cyt}}}{dt} = \text{vol}_{\text{cyt}} G_{\text{O}_2^-} - \frac{A}{2} P_{\text{O}_2^-} [\text{O}_2^-]_{\text{cyt}} \left(\frac{\zeta}{1 - e^{-\zeta}} \right) - \text{vol}_{\text{cyt}} k_{\text{NO}, \text{O}_2^-} [\text{NO}]_{\text{cyt}} [\text{O}_2^-]_{\text{cyt}} \quad (8)$$

where

$P_{\text{O}_2^-}$ (estimated as 0.06 cm/s) is the cell membrane permeability to O_2^- ; because O_2^- is charged, the diffusion term depends on the nondimensional transmembrane electric potential difference, given by $\zeta = -FV_m/RT$. The volumetric generation rate of O_2^- ($G_{\text{O}_2^-}$) is taken to vary with the luminal pressure P (in mmHg) when the latter is >100 mmHg:

$$G_{\text{O}_2^-} = \begin{cases} G_{\text{O}_2^-}^* \alpha_{\text{O}_2^-}, & P < 100 \text{ mmHg}, \\ G_{\text{O}_2^-}^* \alpha_{\text{O}_2^-} \left(1 + \beta_{\text{O}_2^-} \left(\frac{P-100}{40} \right) \right), & P \geq 100 \text{ mmHg} \end{cases} \quad (9)$$

Ren et al. (46) reported that pressure-induced increases in O_2^- were fourfold greater in SHR afferent arterioles compared with WKY afferent arterioles (48 vs. 12%, as perfusion pressure increased from 60 to 140 mmHg). Moreover, the basal rate of O_2^- synthesis is higher in hypertensive rats (37). Given these observations, the parameters

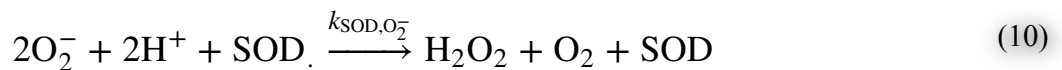
$\alpha_{\text{O}_2^-}$ and

$\beta_{\text{O}_2^-}$ are set to 1.0 and 0.12, respectively, for normotensive rats, and to 2.5 and 0.48, respectively, for SHR.

The reference generation rate

$G_{\text{O}_2^-}^*$ is taken as 14.4 $\mu\text{M/s}$.

The two sinks for O_2^- include its reaction with NO to form ONOO^- (Eq. 7) and the reaction catalyzed by superoxide dismutase (SOD) to form H_2O_2 :



The reaction rate is given by the product

$k_{\text{SOD}, \text{O}_2^-} [\text{SOD}]_{\text{cyt}} [\text{O}_2^-]_{\text{cyt}}$, where $[\text{SOD}]_{\text{cyt}}$ and

$k_{\text{SOD}, \text{O}_2^-}$ are, respectively, set to 1 μM and $1.6 \times 10^3 \mu\text{M}^{-1} \cdot \text{s}^{-1}$. Owing to insufficient quantitative data, the effects of ONOO^- and H_2O_2 on afferent arteriole vasomotor responses are not considered in this model.

Soluble Guanylate Cyclase Activation and cGMP Generation

Activation of soluble guanylate cyclase by NO. The activation of soluble guanylate cyclase (sGC) by NO is modeled following the approach of Yang et al. (61). First, in a reversible reaction, NO binds to basal sGC (denoted $\text{sGC}_{\text{basal}}$) to yield an intermediate six-coordinate ferrous nitrosyl heme complex (denoted sGC_{6c}). Then, sGC_{6c} is converted to a fully activated five-coordinate complex (denoted sGC_{5c}). This

second step is believed to occur via two single-step irreversible processes, one NO dependent and the other NO independent. Finally, the deactivation of sGC_{5c} is represented as a first-order, irreversible reaction. The kinetic equations are expressed as:

$$\frac{d [sGC_{\text{basal}}]}{dt} = -k_1^{\text{sGC}} [sGC_{\text{basal}}] [\text{NO}] + k_{-1}^{\text{sGC}} [sGC_{6c}] + k_4^{\text{sGC}} [sGC_{5c}] \quad (11)$$

$$\frac{d [sGC_{6c}]}{dt} = +k_1^{\text{sGC}} [sGC_{\text{basal}}] [\text{NO}] - k_{-1}^{\text{sGC}} [sGC_{6c}] - k_2^{\text{sGC}} [sGC_{6c}] - k_3^{\text{sGC}} [sGC_{6c}] [\text{NO}] \quad (12)$$

For simplicity, the subscript “cyt” is omitted in the conservation equations of species other than the main ions, NO, and O₂⁻. The concentration of sGC_{5c} can be determined from the conservation equation:

$$[sGC_{\text{basal}}] + [sGC_{6c}] + [sGC_{5c}] = [sGC]_{\text{tot}} \quad (13)$$

where the total sGC concentration ([sGC]_{tot}) is fixed, since we assume that cytosolic volume remains constant. The reaction rates (k_i^{sGC}) in [Eqs. 11](#) and [12](#) are taken to be constant, with two exceptions. The conversion of sGC_{5c} to basal sGC is assumed to be mediated by cGMP. Thus

$$k_4^{\text{sGC}} = K_4^{\text{sGC}} [\text{cGMP}] \quad (14)$$

where $K_4^{\text{sGC}} = 0.098 \mu\text{M}^{-1} \cdot \text{s}^{-1}$. As discussed below, the production rate of cGMP increases with [sGC_{5c}], which implies a negative feedback loop.

Oxidative stress has been shown to alter the redox state of the prosthetic heme on sGC, such that the latter becomes unresponsive to NO ([53](#)). To account for the inhibitory effects of oxidative stress on NO-mediated activation of sGC, we assume that the rate k_1^{sGC} is reduced by a factor of 10 when [O₂⁻]_{cyt} is above 10 nM (i.e., twice its base-case value).

Generation and degradation of cGMP. The synthesis of cGMP is represented as in Ref. [61](#). GTP is converted to cGMP at a rate that depends on sGC_{5c} levels. Cyclic nucleotide phosphodiesterases (PDE) then hydrolyze cGMP into GMP. That degradation pathway is modeled using Michaelis-Menten kinetics, with the maximum rate taken to be proportional to [cGMP], to account for PDE activation by cGMP. Taken together, the kinetics of cGMP formation is given by:

$$\frac{d [\text{cGMP}]}{dt} = V_{\text{max,sGC}} [sGC_{5c}] - \frac{k_{\text{PDE}} [\text{cGMP}]^2}{K_{\text{M,PDE}} + [\text{cGMP}]} \quad (15)$$

Mechanosensitive Channels

As discussed below, the identity of the mechanosensitive cation channels activated by wall stress that are expressed by the afferent arteriole remains to be fully elucidated. We assume that these channels predominantly carry Na^+ and that they are somewhat permeable to Ca^{2+} but not to other ions. The corresponding currents are calculated as:

$$I_{\text{Na,Pres}} = G_{\text{Na,Pres}}(V_m - E_{\text{Na}}) \quad (16)$$

$$I_{\text{Ca,Pres}} = G_{\text{Ca,Pres}}(V_m - E_{\text{Ca}}) \quad (17)$$

where the conductance $G_{i,\text{Pres}}$ to ion i ($i = \text{Na}^+, \text{Ca}^{2+}$) is taken to depend on the luminal pressure P as follows:

$$G_{i,\text{Pres}} = \begin{cases} G_{i,\text{Pres}}^0 \left(1 + \alpha_{\text{Pres}} \left(\frac{P}{P_1} - 1 \right) \right), & P < P_2 \\ G_{i,\text{Pres}}^0 \left(1 + \alpha_{\text{Pres}} \left(\frac{P}{P_1} - 1 \right) \left(\frac{P}{P_2} \right) \right), & P \geq P_2 \end{cases} \quad (18)$$

with $P_1 \equiv 100$ mmHg. P_2 is set to 60 mmHg, consistent with the finding that the myogenic response becomes ineffective at sufficiently low luminal pressure (7). The base-case value of α_{Pres} , which characterizes the pressure sensitivity of the mechanosensitive channels, is taken as 1.75.

NO and cGMP Effects on K^+ Transport Pathways

As in Ref. 61, the model considers that NO and cGMP can separately shift the voltage dependence of the open probability of Ca^{2+} -activated K^+ (K_{Ca}) channels toward more negative potentials. The current flowing through these channels is calculated as:

$$I_{\text{K,Ca}} = G_{\text{KCa}} P_{\text{KCa}} (V_m - E_{\text{K}}) \quad (19)$$

$$P_{\text{KCa}} = 0.65 P_f + 0.35 P_s \quad (20)$$

$$\frac{dP_f}{dt} = \frac{\bar{P}_{\text{KCa}} - P_f}{\tau_{P_f}} \quad (21)$$

$$\frac{dP_s}{dt} = \frac{\bar{P}_{\text{KCa}} - P_s}{\tau_{P_s}} \quad (22)$$

$$\bar{P}_{KCa} = \frac{1}{1 + \exp\left(-\frac{V_m - V_{KCa}}{k_{KCa}}\right)} \quad (23)$$

$$V_{KCa} = V_{Ca}^{KCa} \log_{10} ([Ca]_{cyt}) - V_{NO}^{KCa} \left(\frac{[NO]}{K_{M,NO}^{KCa} + [NO]} \right) - V_{cGMP}^{KCa} \left(\frac{[cGMP]}{K_{M,cGMP}^{KCa} + [cGMP]} \right) \quad (24)$$

where P_f and P_s denote the fast and slow components of the channel activation process, respectively, and τ_{P_f} and τ_{P_s} denote the corresponding time constants. The steady-state open probability of the channel is given by \bar{P}_{KCa} . Parameter values are given in Table 5 in Ref. [10](#).

O₂⁻ Effects on K⁺ and Na⁺ Transport Pathways

The current across Na⁺-K⁺-ATPase pumps is determined as:

$$I_{NaK} = I_{NaK,max} \left(\frac{[K]_{out}}{[K]_{out} + K_{M,NaK}^K} \right)^2 \left(\frac{[Na]_{cyt}}{[Na]_{cyt} + K_{M,NaK}^{Na}} \right)^3 \quad (25)$$

The pump affinities are taken from Refs. [39](#) and [63](#). To account for the observed inhibitory effects of O₂⁻ on Na⁺-K⁺-ATPase activity ([13](#)), we assume that O₂⁻ modulates the maximum current as:

$$I_{NaK,max} = I_{NaK,max}^* \left[1 - \frac{[O_2^-]_{cyt}}{[O_2^-]_{cyt} + K_{M,O_2^-}^{NaK}} \right] \quad (26)$$

where $K_{M,O_2^-}^{NaK}$ is set to 1.6 μM.

Effects of cGMP, NO, and O₂⁻ on Ca²⁺ Transport Pathways

cGMP-dependent PKG has been found to stimulate PMCA pumps ([62](#)). The current through PMCA is expressed as:

$$I_{PMCA} = I_{PMCA,max} \left(\frac{[Ca]_{cyt}}{K_{M,PMCA}^{Ca} + [Ca]_{cyt}} \right) \quad (27)$$

where

$$I_{PMCA,max} = I_{PMCA,max}^* \left(1 + 0.1 \frac{[cGMP]}{K_{M,cGMP}^{PMCA} + [cGMP]} \right) \quad (28)$$

The maximum current in the absence of cGMP, $I_{PMCA,max}^*$, is taken as 4.5 pA. The affinities for Ca^{2+} ($K_{M,PMCA}^{Ca}$) and for cGMP ($K_{M,cGMP}^{PMCA}$) are taken as 0.170 μ M (18) and 1.0 μ M (10), respectively. To obtain a better fit with afferent arteriole data, we assume a smaller dependence of the PMCA current on cGMP levels than in our descending vasa recta model (10).

At sufficiently high concentrations ($\geq 0.1 \mu$ M), cGMP has been shown to activate SERCA pumps via phosphorylation of phospholamban (5), whereas O_2^- inhibits SERCA (34). The SERCA current is determined as:

$$I_{SERCA} = I_{SERCA,max} \left(\frac{([Ca]_{cyt})^2}{([Ca]_{cyt})^2 + (K_{mf})^2} \right) \quad (29)$$

where

$$K_{mf} = K_{mf}^* \left(1 - \frac{1}{2} \frac{[cGMP]}{K_{M,cGMP}^{SERCA} + [cGMP]} \right) \quad (30)$$

where $K_{M,cGMP}^{SERCA}$ is set to 0.50 μ M (5) and K_{mf}^* is taken as 0.59 μ M (10). The inhibitory effects of O_2^- are captured in the maximum SERCA current term:

$$I_{SERCA,max} = I_{SERCA,max}^* \left(1 - \frac{([O_2^-]_{cyt})^{0.5}}{(K_{M,O_2^-}^{SERCA})^{0.5} + ([O_2^-]_{cyt})^{0.5}} \right) \quad (31)$$

The maximum current,

$I_{SERCA,max}^*$, is taken as 11.8 pA and

$K_{M,O_2^-}^{SERCA}$ as 20 μ M (12).

The current across L-type Ca^{2+} channels ($Ca_V1.2$) is given by:

$$I_{Ca,L} = G_{Ca,L} p_o (V_m - E_{Ca}) \quad (32)$$

where $G_{Ca,L}$ represents the maximum conductance of the channel, and p_o , which denotes the open state of the channel, is determined using the model of Faber et al. (15). Model equations can be found in Ref. 11. Several studies have shown that reactive oxygen species (ROS) stimulate L-type Ca^{2+} channel activity (1, 24). Thus we assume that the maximum conductance of the channel is dependent on cytosolic $[O_2^-]$ above a certain threshold:

$$G_{Ca,L} = \begin{cases} G_{Ca,L}^* & [O_2^-]_{cyt} < [O_2^-]_{100} \\ G_{Ca,L}^* \left(1 + \beta_{Ca,L} \left(\frac{[O_2^-]_{cyt}}{[O_2^-]_{100}} - 1 \right) \right) & [O_2^-]_{cyt} \geq [O_2^-]_{100} \end{cases} \quad (33)$$

where $[O_2^-]_{100}$ (taken as 5.0 nM) corresponds to the predicted cytosolic concentration of superoxide in normotensive rats at a luminal pressure of 100 mmHg. Based on the data of Smirnov et al. (52) and this model, the reference maximum conductance of the L-type channel ($G_{Ca,L}^*$) is estimated as 0.5 nS/pF or 2.75 nS. The base-case value of $\beta_{Ca,L}$ is taken as 0.10.

MLCK- and MLCP-Dependent Phosphorylation of Myosin

The fraction of myosin cross bridges that are phosphorylated determines the contractile force. Following the approach of Yang et al. (61), we consider four species: free cross bridges (Myo), phosphorylated cross bridges (MyoP), attached phosphorylated, cycling cross bridges (AMyoP), and attached dephosphorylated, noncycling cross bridges (AMyo). The concentration of these MLC species is calculated as:

$$\frac{d [Myo]}{dt} = -k_1^{Myo} [Myo] + k_2^{Myo} [MyoP] + k_7^{Myo} [AMyo] \quad (34)$$

$$\frac{d [MyoP]}{dt} = +k_1^{Myo} [Myo] - k_2^{Myo} [MyoP] - k_3^{Myo} [MyoP] + k_4^{Myo} [AMyoP] \quad (35)$$

$$\frac{d [AMyoP]}{dt} = +k_3^{Myo} [MyoP] - k_4^{Myo} [AMyoP] - k_5^{Myo} [AMyoP] + k_6^{Myo} [AMyo] \quad (36)$$

$$[Myo] + [MyoP] + [AMyoP] + [AMyo] = [Myo]_{tot} \quad (37)$$

The rate constants k_3^{Myo} , k_4^{Myo} , and k_7^{Myo} are fixed (60). The rate constants k_1^{Myo} and k_6^{Myo} represent the activity of MLCK, and are taken to be proportional to the fraction of the fully activated form of the enzyme (the one that is bound to calmodulin and 4 Ca^{2+} ions):

$$k_1^{\text{Myo}} = k_6^{\text{Myo}} = k_{\text{MLCK}}^{\text{Myo}} \frac{[\text{MLCK} \cdot \text{CaM} \cdot \text{Ca}_4]}{[\text{MLCK}]_{\text{tot}}} \quad (38)$$

where $k_{\text{MLCK}}^{\text{Myo}}$ has a fixed value of 0.2135 s^{-1} .

The rate constants k_2^{Myo} and k_5^{Myo} represent the activity of MLCP. cGMP has been shown to indirectly activate MLCP, which may underlie the observed cGMP-induced Ca^{2+} desensitization in vasodilation (35). The cGMP effects are accounted for as:

$$k_2^{\text{Myo}} = k_5^{\text{Myo}} = k_{\text{MLCP}}^{\text{Myo}} f_{\text{MLCP}}^{\text{act}} \left(1 + 0.1 \frac{[\text{cGMP}]^2}{(K_{\text{M,cGMP}}^{\text{MLCP}})^2 + [\text{cGMP}]^2} \right) \quad (39)$$

where $k_{\text{MLCP}}^{\text{Myo}}$ is a constant (set to 0.70 s^{-1}), $f_{\text{MLCP}}^{\text{act}}$ is the fraction of active (dephosphorylated) MLCP, and $K_{\text{M,cGMP}}^{\text{MLCP}}$ is taken as $5.5 \text{ }\mu\text{M}$ (61). MLCP is also negatively regulated by Rho kinase (RhoK). The fraction $f_{\text{MLCP}}^{\text{act}}$ is determined following the approach of Mbikou et al. (41):

$$\frac{df_{\text{MLCP}}^{\text{act}}}{dt} = k_{-P} - (k_{+P} + k_{-P}) f_{\text{MLCP}}^{\text{act}} \quad (40)$$

The dephosphorylation rate k_{-P} is taken to remain constant (0.2 s^{-1}), whereas the phosphorylation rate k_{+P} varies with the fraction of active RhoK ($f_{\text{RhoK}}^{\text{act}}$) as:

$$k_{+P} = \frac{k_{\text{catP}}}{K_{\text{MP}}} f_{\text{RhoK}}^{\text{act}} [\text{RhoK}]_{\text{tot}} \quad (41)$$

where k_{catP} (2.5 s^{-1}) and K_{MP} ($2.5 \text{ }\mu\text{M}$) are the corresponding enzyme-substrate breakdown constant and Michaelis constant, respectively, and $[\text{RhoK}]_{\text{tot}}$ is the total concentration of RhoK (fixed at $2.0 \text{ }\mu\text{M}$) (41). In turn, the fraction of active RhoK is given by:

$$\frac{df_{\text{RhoK}}^{\text{act}}}{dt} = k_{+RK} - (k_{+RK} + k_{-RK}) f_{\text{RhoK}}^{\text{act}} \quad (42)$$

where the “off” rate constant k_{-RK} is set to 0.1 s^{-1} . The activation of RhoK is Ca^{2+} dependent and the “on” rate constant k_{+RK} is calculated as:

$$k_{+RK} = \gamma_{RK}[\text{Ca}]_{\text{cyt}} \quad (43)$$

where γ_{RK} is taken as $0.3 \mu\text{M} \cdot \text{s}^{-1}$ in normotensive rats (41). There is evidence that oxidative stress activates RhoA/RhoK signaling in vascular smooth muscle cells (3, 31, 32), but the underlying signaling cascades remain to be fully characterized. To incorporate these ROS-dependent effects in the present study, we simply assume that γ_{RK} is multiplied by a factor of 1.5 when $[\text{O}_2^-]_{\text{cyt}}$ is $>10 \text{ nM}$.

Vessel Mechanics

Variations in the number of cross bridges induce variations in the contractile force, which in turn modulate the arteriolar diameter. To simulate vasomotion, the model represents the vascular wall tension as the sum of a passive component, T_{pass} , and an active myogenic component, given by the product of the maximal active tension that is generated at a given vessel circumference, $T_{\text{act}}^{\text{max}}$, and the fraction of MLC that is phosphorylated. Thus, the total tension in the wall T_{wall} is given by:

$$T_{\text{wall}} = T_{\text{pass}} + \left(\frac{[\text{MyoP}] + [\text{AMyoP}]}{[\text{Myo}]_{\text{tot}}} \right) T_{\text{act}}^{\text{max}} \quad (44)$$

The passive tension is a function of the afferent arteriole diameter D :

$$T_{\text{pass}} = C_{\text{pass}}'' + C_{\text{pass}} \exp \left(C_{\text{pass}}' \left(\frac{D}{D_0} - 1 \right) \right) \quad (45)$$

where D_0 denotes the reference arteriolar diameter. The maximal active tension is given by:

$$T_{\text{act}}^{\text{max}} = C_{\text{act}} \exp \left(- \left(\frac{D/D_0 - C_{\text{act}}'}{C_{\text{act}}''} \right)^2 \right) \quad (46)$$

The vessel diameter changes according to the difference between the tension T_{pres} resulting from intravascular pressure p , given by $T_{\text{pres}} = PD/2$, and the tension generated within the wall, T_{wall} :

$$\frac{dD}{dt} = \frac{1}{\tau_d} (T_{\text{pres}} - T_{\text{wall}}) \quad (47)$$

where τ_d is a time constant. Parameter values for the muscle mechanics model are given in [Table 1](#). Parameter values related to NO, cGMP, and O_2^- are given above. Other parameter values can be found in Refs. [10](#) and [11](#), with the following modifications: $G_{\text{ClCa}} = 0.48$ nS, $K_{\text{ClCa}} = 100$ nM, and $v_{\text{RyR}} = 14$ s⁻¹.

MODEL RESULTS

We examined the response of the rat afferent arteriole to NO, O_2^- , angiotensin II (ANG II), and perfusion pressure in normotensive and SHR. Parameter values that differ between these strains are summarized in [Table 2](#) and discussed below.

Effects of Superoxide on the Basal Diameter of the Afferent Arteriole

When the luminal pressure is set to its base-case value of 100 mmHg, the model predicts spontaneous vasomotion. In normotensive rats, the cytosolic concentration of Ca^{2+} (denoted $[\text{Ca}^{2+}]_{\text{cyt}}$ below) oscillates between 180 and 320 nM, with a frequency of 145 mHz. The cytosolic concentration of NO ($[\text{NO}]_{\text{cyt}}$) and O_2^- ($[\text{O}_2^-]_{\text{cyt}}$) equals 152 and 4.9 nM, respectively. The average afferent arteriole luminal diameter is 20.5 μm , with an oscillation amplitude of ~ 1.9 μm .

The superoxide production rate in hypertensive rats is taken to be 2.5 times greater than that of normotensive rats ([37](#)). Thus, in SHR, the predicted values of $[\text{NO}]_{\text{cyt}}$ and $[\text{O}_2^-]_{\text{cyt}}$ are 100 and 14 nM, respectively. Cytosolic Ca^{2+} oscillations are almost negligible: $[\text{Ca}^{2+}]_{\text{cyt}}$ varies between 272 and 274 nM. The arteriolar luminal diameter is 17.1 μm , that is, significantly lower than in normotensive rats, as observed experimentally ([20](#), [46](#), [51](#)).

In this model, elevated superoxide levels modulate Ca^{2+} signaling in several ways: by raising the conductance of L-type Ca^{2+} channels ($G_{\text{Ca,L}}$), by rendering basal sGC less responsive to NO, by scavenging NO, and by activating RhoK, which in turn inactivates MLCP. To determine the relative contribution of these mechanisms to the reduced diameter in SHR, we abolished each effect separately. When $G_{\text{Ca,L}}$ was maintained at its reference (normotensive) value, the afferent arteriolar diameter in SHR was computed as 18.4 μm ; when the rate of NO scavenging by O_2^- was kept at its normotensive value, the diameter was 17.6 μm ; without ROS-induced sGC desensitization to NO, the diameter was 17.4 μm ; lastly, without ROS-mediated activation of RhoK, it was 18.1 μm . Thus ROS-induced modulation of $G_{\text{Ca,L}}$ is predicted to be the dominant mechanism by which superoxide affects vasoconstriction.

Effects of NO Synthase Inhibition and Tempol

NO and its second messenger cGMP favor vasodilation by maintaining low levels of Ca^{2+} and MLC phosphorylation. They do so by stimulating Ca^{2+} uptake from the cytosol into the SR (via SERCA pumps) and Ca^{2+} efflux into the extracellular space (via PMCA pumps), activating K_{Ca} channels to induce hyperpolarization, and enhancing MLCP activity ([Fig. 1](#)). Our model predicts that when NO synthesis is fully inhibited, spontaneous vasomotion is abolished and the luminal diameter decreases to 16.0 μm in

normotensive rats, a 22% reduction that is close to the measured value (18%) in Sprague-Dawley (SD) rats treated with *N*-nitro-*L*-arginine (27). In SHR, NOS inhibition is also predicted to reduce the diameter from 17.1 to 14.5 μm ; this 15% decrease is identical to in vitro findings (26).

Experimental studies have found that the SOD mimetic Tempol (100 μM) has no significant effect on the afferent arteriole of normotensive rats under basal conditions (26, 50). We simulated the addition of Tempol by increasing the concentration of SOD from 1 to 100 μM . As observed experimentally, at the baseline pressure of 100 mmHg, the model predicts that Tempol has little impact on the arteriolar diameter in normotensive rats, because O_2^- levels are too low to significantly affect NO concentrations and Ca^{2+} signaling pathways. In SHR, Tempol is predicted to increase the arteriolar diameter (by 25%), as seen in many studies (47, 48, 26), albeit with exceptions (46).

We also performed simulations in which we eliminated the downstream effects of NO and cGMP one by one, so as to assess the contribution of each mechanism to the maintenance of basal tone in normotensive rats. Results are summarized in Fig. 2. Abolishing cGMP-induced stimulation of MLCP does not affect $[\text{Ca}^{2+}]_{\text{cyt}}$ but reduces the basal arteriolar diameter by 0.6 μm . Abolishing the direct and indirect effects of NO on K_{Ca} channels slightly depolarizes the smooth muscle cell, raises the average $[\text{Ca}^{2+}]_{\text{cyt}}$ by ≈ 15 nM, and reduces the arteriolar diameter by 1.7 μm . Eliminating cGMP-induced activation of PMCA has a larger impact: it lowers the diameter by 2.3 μm . Lastly, in the absence of cGMP-mediated effects on SERCA, calcium oscillations vanish and $[\text{Ca}^{2+}]_{\text{cyt}}$ remains constant. Even though the rate of Ca^{2+} uptake into the SR is then reduced compared with its average base-case value, $[\text{Ca}^{2+}]_{\text{cyt}}$ is slightly lower than its average base-case value, owing to nonlinear effects (i.e., the interplay between Ca^{2+} uptake into/release from the SR). As a result, the predicted arteriolar diameter is 0.4 μm higher than the average diameter in the base case.

Effects of ANG II

We simulated the effects of ANG II by increasing the generation rate of IP_3 and O_2^- twofold and lowering the conductance of K^+ channels by 60% (12, 54). With these assumptions, the model predicts that ANG II abolishes vasomotion and reduces the arteriolar diameter to 13.2 μm in normotensive rats (a 36% decrease) and 12.4 μm in SHR. Measured values of the fractional diameter decrease induced by ANG II range from 20 to 60% in SD, depending on the concentration of ANG II (27, 50, 55).

In vitro, NOS inhibition enhances ANG II-induced vasoconstriction. Ikenaga et al. (27) observed that in SD juxtamedullary arterioles 10 nM ANG II reduced the arteriolar lumen by 35%; in the presence of *N*-nitro-*L*-arginine, the same concentration of ANG II lowered the diameter by 50%. Our model predicts similar trends: in the presence of ANG II and with full NOS inhibition, the predicted arteriolar diameter is 12.4 μm in normotensive rats, a 40% reduction from the base-case value (Fig. 3).

Conversely, NO donors have been shown to reverse ANG II-induced vasoconstriction. At 900 nM, NO was found to abolish almost entirely the effects of ANG II in SD rats (55). In accordance with these experimental results, our model predicts that in the presence of ANG II and a NO donor yielding $[\text{NO}]_{\text{cyt}} = 900$ nM, the arteriolar diameter is 18.0 μm in normotensive rats, that is, 88% of its baseline value (Fig. 3).

Effects of Luminal Pressure Increases

Increases in luminal pressure are thought to elicit vasoconstriction via a signaling cascade that involves the opening of nonselective, mechanosensitive cation channels and the subsequent depolarization of the smooth muscle cell, followed by Ca^{2+} entry through voltage-gated channels (42). Several theoretical studies, including our previous model of the myogenic response in the rat afferent arteriole, have demonstrated the plausibility of this mechanism (4, 11). The present model, in addition, accounts for recent evidence that ROS production increases in response to elevated pressure (46, 56). In this model, the O_2^- generation rate is taken to increase linearly with pressure beyond 100 mmHg (Eq. 9), with a proportionality constant that differs between normotensive and hypertensive rats, based on experimental evidence (46). Since the conductance of L-type Ca^{2+} channels ($G_{\text{Ca,L}}$) is assumed to vary with $[\text{O}_2^-]_{\text{cyt}}$, as observed experimentally (1, 24), changes in perfusion pressure, via their effect on the rate of O_2^- synthesis, modulate $G_{\text{Ca,L}}$.

The pressure dependence of the mechanosensitive channel conductance and the $[\text{O}_2^-]_{\text{cyt}}$ dependence of the L-type channel conductance remain to be fully described. In our model, they are respectively characterized by the proportionality constants α_{PRES} (Eq. 18) and $\beta_{\text{Ca,L}}$ (Eq. 33), which are set to 1.75 and 0.10, respectively, in the base case. Shown in Figs. 4 and 5 are the predicted effects of an increase in luminal pressure on the arteriolar diameter for different values of α_{PRES} and $\beta_{\text{Ca,L}}$.

With base-case parameter values, the model predicts that a step change in pressure from 100 to 160 mmHg lowers the arteriolar diameter by 35% (from 20.5 to 13.3 μm) in normotensive rats, and by 25% (from 17.1 to 12.8 μm) in SHR. In relative terms, pressure-induced changes in diameter are smaller in SHR because the fraction of MLC that is phosphorylated (which determines the vascular radius) becomes less sensitive to changes in $[\text{Ca}^{2+}]_{\text{cyt}}$ as the latter is increased. In normotensive rats, the proportion of MLC that is phosphorylated increases from an average value of 0.31 at 100 mmHg to 0.78 at 160 mmHg; in SHR, it increases from 0.42 at 100 mmHg to 0.85 at 160 mmHg. Thus the up-step in pressure elicits a proportionally smaller change in radius in the latter strain.

As depicted in Fig. 4, the amplitude of the myogenic response predicted by the model depends significantly on the value of α_{PRES} . If α_{PRES} is increased 2-fold to 3.50, raising the luminal pressure from 100 to 160 mmHg lowers the arteriolar diameter by 39% in normotensive rats and 27% in SHR. Conversely, if α_{PRES} is set to half its base-case value, the corresponding diameter reductions are 28 and 22%, respectively.

In normotensive rats, pressure variations induce very small changes in $[\text{O}_2^-]_{\text{cyt}}$; thus the myogenic response is unaffected by the value of $\beta_{\text{Ca,L}}$ (which characterizes the $[\text{O}_2^-]_{\text{cyt}}$ dependence of the L-type channel conductance). In SHR, by contrast, pressure variations elicit large changes in $[\text{O}_2^-]_{\text{cyt}}$. Hence, changes in $\beta_{\text{Ca,L}}$ significantly modulate the arteriolar diameter in SHR, more so at 100 mmHg than at 160 mmHg (Fig. 5). Indeed, as described above, the fraction of MLC that is phosphorylated is more sensitive to changes in the cytosolic concentration of Ca^{2+} at low luminal pressures (when $[\text{Ca}^{2+}]_{\text{cyt}}$ is on the order of 300 nM in SHR) than at high luminal pressures (when $[\text{Ca}^{2+}]_{\text{cyt}}$ is $>1 \mu\text{M}$ in SHR). Thus raising $\beta_{\text{Ca,L}}$ (and therefore $[\text{Ca}^{2+}]_{\text{cyt}}$) has a greater constricting effect at 100 mmHg than at 160 mmHg. As a consequence, the relative decrease in diameter following an up-step in pressure diminishes as $\beta_{\text{Ca,L}}$ increases.

Overall, our results indicate that the parameter α_{PRES} has a stronger impact on model predictions than $\beta_{\text{Ca,L}}$. In the remaining simulations, $\beta_{\text{Ca,L}}$ is fixed at 0.10.

Several investigators have examined the myogenic response of the afferent arteriole in SD and WKY rats. In isolated perfused hydronephrotic SD kidneys, Loutzenhiser et al. (38) measured a 36% reduction in the arteriolar diameter following a step change in pressure from 80 to 160 mmHg. Using the blood-perfused juxtamedullary nephron technique, Sharma et al. (50) found that the arteriolar diameter decreased by 11 and 27% when the pressure was increased from 100 to 130 and 160 mmHg, respectively. In other studies, however, the myogenic response was much smaller. In isolated afferent arterioles, Ren et al. (46) found that raising the luminal pressure from 80 to 140 mmHg reduced the vessel diameter by 10% in WKY; similar results were obtained in SD. Using the juxtamedullary nephron technique, Imig et al. (28) reported an 8% decrease in arteriolar diameter when the perfusion pressure was raised from 80 to 160 mmHg. With base-case parameter values, our model yields a significant myogenic response, in agreement with the first set of studies. A smaller response can be predicted if α_{PRES} is lowered (Fig. 4).

We also simulated the effects of adding Tempol (100 μM) on the myogenic response. In agreement with experimental observations (50), our model predicts that Tempol (100 μM) has negligible effects ($<1 \mu\text{m}$) on the myogenic response in normotensive rats, independently of the value of α_{PRES} .

In the study of Ren et al. (46), SHR exhibited a stronger myogenic response than WKY. The arteriolar diameter in SHR was reduced by 17–21 and 24–32% as luminal pressure was increased from 100 to 120 and 140 mmHg, respectively; these changes were accompanied by an increase in ROS production (46). Ito et al. (29) reported a comparable 34% diameter decrease in SHR when pressure was elevated from 80 to 140 mmHg. With base-case parameter values, our model predicts slightly lower values: raising luminal pressure from 100 to 120 and 140 mmHg elicits a 16 and 23% decrease in diameter, respectively (Fig. 4). If α_{PRES} is increased twofold, corresponding changes are 22 and 27%, i.e., within the range of the first study.

The predicted effects of Tempol on the myogenic response of SHR are shown in Fig. 6. In these simulations, α_{PRES} is set to either 1.75 (its base-case value) or 3.5. The model correctly predicts that Tempol significantly attenuates pressure-induced vasoconstriction in SHR. However, in contradiction with the findings of Ren et al. (46), the effects of Tempol are found to decrease with increasing luminal pressure. Possible reasons for this discrepancy are discussed below.

DISCUSSION

We developed the present model to understand how NO and superoxide modulate the diameter of the renal afferent arteriole and its myogenic response. To do so, we expanded our previous model of the afferent arteriole vascular smooth muscle cell to include 1) the kinetics of NO and O_2^- formation, diffusion, and reaction, 2) the effects of NO and its second messenger cGMP on Ca^{2+} uptake and efflux into the cell, on K_{Ca} channel currents, and on MCLP activity, and 3) the impact of O_2^- on Na^+/K^+ -ATPase pumps, SERCA, L-type Ca^{2+} channels, as well as RhoK and the NO sensitivity of sGC (Fig. 1).

We formulated a set of assumptions to obtain good agreement between model predictions and experimental measurements under a variety of conditions and for normotensive and spontaneously hypertensive rats. The key assumptions, which are based on experimental findings, are that 1) a rise in perfusion pressure elicits an increase in O_2^- production, and 2) O_2^- in turn regulates the conductance of L-type Ca^{2+} channels. In the absence of specific data, we assumed a linear dependence for both functions ([Eqs. 9](#) and [33](#)). With these assumptions, our model is able to adequately replicate a number of experimental findings regarding the effects of NOS inhibition, Tempol, ANG II, and variations in luminal pressure on the arteriolar diameter in normotensive and hypertensive rats, with a few caveats as discussed below.

When we simulated the full inhibition of NOS in normotensive rats, spontaneous vasomotion disappeared, whereas oscillations are maintained ([55](#)) or augmented ([58](#)) in perfused kidney preparations. One possible explanation for this discrepancy regards the effects of NO on SERCA. As illustrated in [Fig. 2](#), when we eliminated the downstream effects of NO and cGMP one by one, oscillations were preserved, except when the effects of cGMP on the affinity of SERCA to Ca^{2+} (K_{mf}) were removed. We also observed that when we accounted for all the effects of NOS inhibition but set K_{mf} to 250 nM (vs. 307 nM in the base case, and 589 nM in the absence of cGMP), spontaneous vasomotion was preserved; the arteriolar diameter oscillated around 15.8 μm with an amplitude of 1.3 μm . It is therefore possible that the model does not properly account for the effects of cGMP on SERCA, i.e., that findings in rat aortic smooth muscle cells ([5](#)) cannot be extrapolated to renal afferent arterioles.

Validating the model by comparing its myogenic response predictions with in vivo or in vitro data is made difficult by the variability of experimental results. As described in MODEL RESULTS, the magnitude of the myogenic response in SD and WKY rats differs significantly between studies, even when similar preparations are used ([28](#), [38](#), [46](#), [50](#)). Moreover, whether SHR have a stronger response than normotensive rats remains unclear. Studies in isolated afferent arterioles suggest that pressure-induced constriction is enhanced in SHR ([29](#), [46](#)), but other investigations, performed on isolated perfused kidneys, indicate that the autoregulatory response of the afferent arteriole is similar in SHR and WKY ([21](#), [45](#)). Additionally, several investigations indicate that Tempol induces vasodilation of the afferent arteriole in SHR at normal perfusion pressures ([8](#), [17](#), [26](#)), but at least one study found no effect of Tempol on the basal arteriolar diameter of these rats ([46](#)).

As we previously discussed ([11](#)), the mechanisms underlying mechanotransduction in vascular smooth muscle cells have yet to be fully understood. The nature of the channels that sense variations in luminal pressure remains uncertain. Our model assumes that pressure changes first activate a channel that carries predominantly Na^+ and Ca^{2+} , with a 20:3 Na^+ -to- Ca^{2+} conductance ratio. The pressure-dependence of this conductance is characterized by a proportionality constant α_{Pres} . Our results indicate that, for a given value of α_{Pres} , fractional changes in arteriolar diameter induced by pressure elevations are smaller in SHR than in normotensive rats. This is because the sensitivity to $[Ca^{2+}]_{cyt}$ variations of the phosphorylated fraction of MLC decreases with increasing $[Ca^{2+}]_{cyt}$ and basal values of $[Ca^{2+}]_{cyt}$ are significantly higher in SHR than in normotensive rats. If indeed the myogenic response of SHR is stronger than that of WKY, our simulations suggest that this could be explained by a higher conductance of mechanosensitive channels in the former.

Our model predicts that Tempol has a mild impact on the myogenic response of SHR at high luminal pressures, whereas Ren et al. (46) observed that Tempol exerted greater effects at large pressure values. In our model, the mechanosensitive channel conductance is unaffected by the presence of Tempol and remains elevated at high pressures; as a result, intracellular Ca^{2+} levels stay high, which favors vasoconstriction. Thus this discrepancy could indicate that mechanosensitive channels are sensitive to ROS and/or NO levels. There is evidence that O_2^- and NO, most likely via their product peroxynitrite, modulate mechanosensitive channels in ventricular myocytes (9), but the underlying mechanisms have not been determined. If we assume that the mechanosensitive channel conductance increases when $[\text{O}_2^-]_{\text{cyt}}$ is elevated, the myogenic response in SHR is then enhanced, but this does not affect the predicted arteriolar diameter in the presence of Tempol. Conversely, if we assume that the mechanosensitive channel conductance is significantly reduced when $[\text{O}_2^-]_{\text{cyt}}$ is low (<1 nM), adding Tempol leads to greater vasodilation in SHR; however, if the mechanosensitive channel conductance is similarly reduced in normotensive rats, Tempol should then exert significant vasodilatory effects in these rats too, which contradicts experimental findings. Further experimental characterization of mechanosensitive channels and their regulation by NO and ROS would be helpful. We should also acknowledge that our assumption that SHR and normotensive rats differ only by their superoxide levels may be too simplistic; other differences between the two strains, such as varying levels of cyclooxygenase-derived products (16), are likely to influence their contractile responses.

The cytosolic concentration of superoxide in vascular smooth muscle cells has not been measured, to our knowledge. We adjusted its production rate to obtain O_2^- concentrations in the nanomolar range (Table 3) and took into consideration the effects of ANG II and perfusion pressure on O_2^- synthesis, but we should recognize this uncertainty. Our estimate of the plasma membrane permeability to NO (P_{NO}) is equally unsure. Based on the measured value of the NO diffusion coefficient in octanol (40), and assuming a membrane thickness of 1 μm , P_{NO} is estimated as 0.03 cm/s. With this hypothesis, the model predicts that, in normotensive rats, most of the NO that enters the afferent arteriole smooth muscle cell from the endothelium diffuses out on the other side. The fraction of NO that instead reacts with O_2^- is 28% in normotensive rats, vs. 53% in SHR (at 100 mmHg). Conversely, the fraction of O_2^- that is scavenged by NO and SOD is, respectively, 35 and 55% in normotensive rats, and 26 and 62% in SHR. In comparison, in the rabbit aorta, the fraction of produced NO that is consumed by chemical reaction has been estimated as 37% (40).

Based on experimental evidence, the model assumes that O_2^- modulates the current across Na^+ - K^+ -ATPase and SERCA only when its concentration is in the micromolar range; in the scenarios examined here, $[\text{O}_2^-]_{\text{cyt}}$ remains below 100 nM and therefore has negligible effects on these two currents. Under these conditions, O_2^- acts in the following ways: by modulating the conductance of L-type Ca^{2+} channels, by activating RhoK (which in turn inactivates MLCP), by scavenging NO, and by lowering the responsiveness of sGC to NO; the latter two mechanisms counteract NO-mediated changes in $[\text{Ca}^{2+}]_{\text{cyt}}$ and MLC phosphorylation. As shown in Table 3, the NO-independent effects of O_2^- seem to predominate in the scenarios we considered: per se (e.g., at a given perfusion pressure), changes in O_2^- production are predicted to have a much greater impact on $G_{\text{Ca,L}}$ than on NO signaling pathways. Stated differently, if the rate of NO scavenging by O_2^- were the same in SHR as in normotensive rats, the SHR afferent arteriolar diameter would only be 0.5 μm higher than its base-case value; i.e., the reduced diameter in SHR does not

appear to stem mostly from NO scavenging. These predictions accord with experimental observations suggesting that elevated renal resistance in SHR is unlikely to stem from ROS-induced quenching of NO (8).

The present model represents a single afferent arteriole smooth muscle cell with a baseline luminal pressure of 100 mmHg. However, luminal hydrostatic pressure decreases along the afferent arteriole, from ~100 mmHg at the inlet to ~50 mmHg at the glomerular end. To represent a segment of the afferent arteriole that is closer to the glomerulus and is thus typically affected by a substantially lower hydrostatic pressure, the myogenic response (Eq. 18) could be modified. More specifically, the parameters P_1 and P_2 in Eq. 18 could be chosen as a function of baseline pressure, so that the same absolute pressure change would induce the same change in conductance ($G_{i,Pres}$), regardless of the baseline hydrostatic pressure. This approach allows one to represent smooth muscle cells at differing locations of the afferent arteriole. A model of an afferent arteriole could then be built by connecting a series of these cell models, coupled via their gap junctions, as in Ref. 49. In conclusion, our mathematical model supports the hypothesis that, per se, increased O_2^- production in the afferent arteriole of SHR substantially alters the myogenic response of the arteriole. Our results also suggest that the constrictive effects of superoxide are not predominantly due to its scavenging of NO, but mostly stem from the NO-independent action of O_2^- on L-type Ca^{2+} channels and RhoK signaling.

GRANTS

This research was supported by National Institute of Diabetes and Digestive and Kidney Diseases Grant DK-089066 and National Science Foundation Grant DMS-1263995.

DISCLOSURES

No conflicts of interest, financial or otherwise, are declared by the author(s).

AUTHOR CONTRIBUTIONS

Author contributions: A.T.L. and A.E. conception and design of research; A.T.L. and A.E. performed experiments; A.T.L. and A.E. analyzed data; A.T.L. and A.E. interpreted results of experiments; A.T.L. and A.E. prepared figures; A.T.L. and A.E. drafted manuscript; A.T.L. and A.E. edited and revised manuscript; A.T.L. and A.E. approved final version of manuscript.

REFERENCES

1. Amberg GC, Earley S, Glapa SA. Local regulation of arterial L-type calcium channels by reactive oxygen species. *Circ Res* 107: 1002–1010, 2010. [PMCID: PMC2967383] [PubMed: 20798361]
2. Beswick RA, Dorrance AM, Leite R, Webb RC. NADH/NADPH oxidase and enhanced superoxide production in the mineralocorticoid hypertensive rat. *Hypertension* 38: 1107–1111, 2001. [PubMed: 11711506]
3. Broughton BR, Jernigan NL, Norton CE, Walker BR, Resta TC. Chronic hypoxia augments depolarization-induced Ca^{2+} sensitization in pulmonary vascular smooth muscle through superoxide-dependent stimulation of RhoA. *Am J Physiol Lung Cell Mol Physiol* 298: L232–L242, 2010.

[PMCID: PMC2822557] [PubMed: 19897743]

4. Carlson BE, Beard DA. Mechanical control of cation channels in the myogenic response. *Am J Physiol Heart Circ Physiol* 301: H331–H343, 2011. [PMCID: PMC3154678] [PubMed: 21572020]
5. Cornell TL, Pryzwansky KB, Wyatt TA, Lincoln TM. Regulation of sarcoplasmic reticulum protein phosphorylation by localized cyclic GMP-dependent protein kinase in vascular smooth muscle cells. *Mol Pharmacol* 40: 923–931, 1991. [PubMed: 1836834]
6. Cowley AW Jr, Mori T, Mattson D, Zou AP. Role of renal NO production in the regulation of medullary blood flow. *Am J Physiol Regul Integr Comp Physiol* 284: R1355–R1369, 2003. [PubMed: 12736168]
7. Cupples WA, Braam B. Assessment of renal autoregulation. *Am J Physiol Renal Physiol* 292: F1105–F1123, 2007. [PubMed: 17229679]
8. de Richelieu LT, Sorensen CM, Holstein-Rathlou NH, Salomonsson M. NO-independent mechanism mediates tempol-induced renal vasodilation in SHR. *Am J Physiol Renal Physiol* 289: F1227–F1234, 2005. [PubMed: 16033921]
9. Dyachenko V, Rueckschloos U, Isenberg G. Modulation of cardiac mechanosensitive ion channels involves superoxide, nitric oxide and peroxynitrite. *Cell Calcium* 45: 55–64, 2009. [PubMed: 18639930]
10. Edwards A, Cao C, Pallone TL. Calcium mechanisms underlying nitric oxide-induced vasodilation in descending vasa recta. *Am J Physiol Renal Physiol* 300: F441–F456, 2011. [PMCID: PMC3044008] [PubMed: 21084408]
11. Edwards A, Layton AT. Calcium dynamics underlying the afferent arteriole myogenic response. *Am J Physiol Renal Physiol* 306: F34–F48, 2014. [PMCID: PMC3921822] [PubMed: 24173354]
12. Edwards A, Pallone TL. Mechanisms underlying angiotensin II-induced calcium oscillations. *Am J Physiol Renal Physiol* 295: F568–F584, 2008. [PMCID: PMC2519179] [PubMed: 18562632]
13. Elmoselhi AB, Butcher A, Samson SE, Grover AK. Free radicals uncouple the sodium pump in pig coronary artery. *Am J Physiol Cell Physiol* 266: C720–C728, 1994. [PubMed: 8166235]
14. Evans R, Fitzgerald S. Nitric oxide and superoxide in the renal medulla: a delicate balancing act. *Curr Opin Nephrol Hypertens* 14: 9–15, 2005. [PubMed: 15586010]
15. Faber GM, Silva G, Livshitz L, Rudy Y. Kinetic properties of the cardiac L-type Ca^{2+} channel and its role in myocyte electrophysiology: a theoretical investigation. *Biophys J* 92: 1522–1543, 2007. [PMCID: PMC1796810] [PubMed: 17158566]
16. Feletou M, Huang Y, Vanhoutte PM. Endothelium-mediated control of vascular tone: COX-1 and COX-2 products. *Br J Pharmacol* 164: 894–912, 2011. [PMCID: PMC3195913] [PubMed: 21323907]
17. Feng MG, Dukacz SA, Kline RL. Selective effect of tempol on renal medullary hemodynamics in spontaneously hypertensive rats. *Am J Physiol Regul Integr Comp Physiol* 281: R1420–R1425, 2001. [PubMed: 11641111]

18. Furukawa KI, Nakamura H. Characterization of the (Ca²⁺-Mg²⁺)ATPase purified by calmodulin-affinity chromatography from bovine aortic smooth muscle. *J Biochem* 96: 1343–1350, 1984. [PubMed: 6151947]
19. Garvin J, Ortiz P. The role of reactive oxygen species in the regulation of tubular function. *Acta Physiol Scand* 179: 225–232, 2003. [PubMed: 14616238]
20. Gattone II, Evan AP, Willis LR, Luft FC. Renal afferent arteriole in the spontaneously hypertensive rat. *Hypertension* 5: 8–16, 1983. [PubMed: 6848472]
21. Hayashi K, Suzuki H, Saruta T. Nitric oxide modulates but does not impair myogenic vasoconstriction of the afferent arteriole in spontaneously hypertensive rats. Studies in the isolated perfused hydronephrotic kidney. *Hypertension* 25: 1212–1219, 1995. [PubMed: 7768564]
22. Heitzer T, Wenzel U, Hink U, Krollner D, Skatchkov M, Stahl RA, Macharzina R, Bräsen JH, Meinertz T, Münzel T. Increased NAD(P)H oxidase-mediated superoxide production in renovascular hypertension: evidence for an involvement of protein kinase C. *Kidney Int* 56: 252–260, 1999. [PubMed: 9893134]
23. Holstein-Rathlou NH, Marsh DJ. Renal blood flow regulation and arterial pressure fluctuations: a case study in nonlinear dynamics. *Physiol Rev* 74: 637–681, 1994. [PubMed: 8036249]
24. Hool LC. Evidence for the regulation of L-type Ca²⁺ channels in the heart by reactive oxygen species: mechanism for mediating pathology. *Clin Exp Pharmacol Physiol* 35: 229–234, 2008. [PubMed: 18197892]
25. Huie RE, Padmaja S. The reaction of NO with superoxide. *Free Radic Res Commun* 18: 195–199, 1993. [PubMed: 8396550]
26. Ichihara A, Hayashi M, Hirota N, Saruta T. Superoxide inhibits neuronal nitric oxide synthase influences on afferent arterioles in spontaneously hypertensive rats. *Hypertension* 37: 630–634, 2001. [PubMed: 11230347]
27. Ikenaga H, Fallet RW, Carmines PK. Basal nitric oxide production curtails arteriolar vasoconstrictor responses to ANG II in rat kidney. *Am J Physiol Renal Fluid Electrolyte Physiol* 271: F365–F373, 1996. [PubMed: 8770168]
28. Imig JD, Zou AP, Ortiz de Montellano PR, Sui Z, Roman RJ. Cytochrome P-450 inhibitors alter afferent arteriolar responses to elevations in pressure. *Am J Physiol Heart Circ Physiol* 226: H1879–H1885, 1994. [PubMed: 8203587]
29. Ito S, Juncos LA, Carretero OA. Pressure-induced constriction of the afferent arteriole of spontaneously hypertensive rats. *Hypertension* 19, Suppl II: II-164–II-167, 1992. [PubMed: 1735572]
30. Iversen BM, Sekse I, Ofstad J. Resetting of renal blood flow autoregulation in spontaneously hypertensive rats. *Am J Physiol Renal Fluid Electrolyte Physiol* 252: F480–F486, 1987. [PubMed: 3826388]

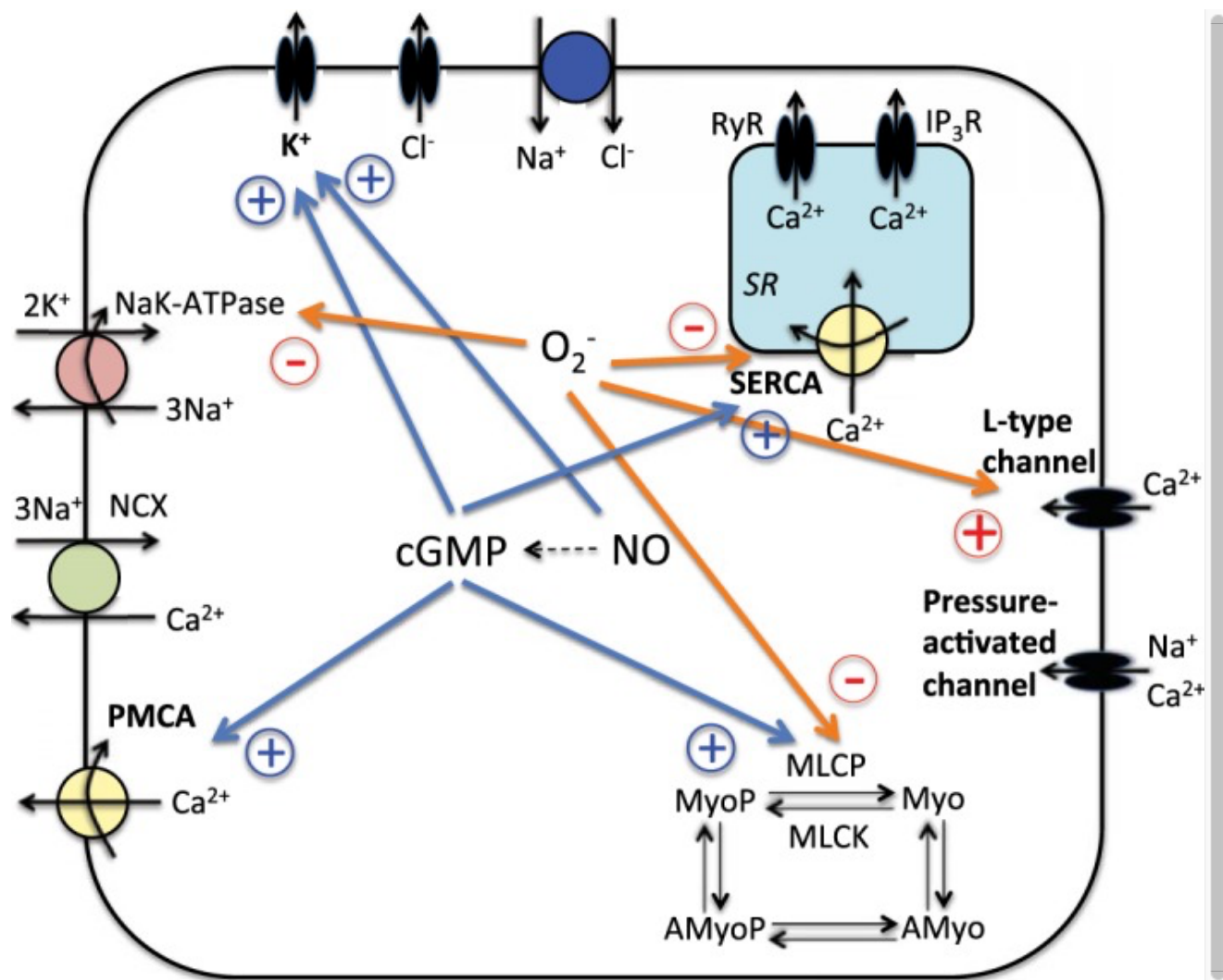
31. Jernigan NL, Walker BR, Resta TC. Reactive oxygen species mediate RhoA/Rho kinase-induced Ca^{2+} sensitization in pulmonary vascular smooth muscle following chronic hypoxia. *Am J Physiol Lung Cell Mol Physiol* 295: L515–L529, 2008. [PMCID: PMC2536792] [PubMed: 18621909]
32. Jin L, Ying Z, Webb RC. Activation of Rho/Rho kinase signaling pathway by reactive oxygen species in rat aorta. *Am J Physiol Heart Circ Physiol* 287: H1495–H1500, 2004. [PubMed: 15371261]
33. Just A. Mechanisms of renal blood flow autoregulation: dynamics and contributions. *Am J Physiol Regul Integr Comp Physiol* 292: R1–R17, 2007. [PubMed: 16990493]
34. Kourie JL. Interaction of reactive oxygen species with ion transport mechanisms. *Am J Physiol Cell Physiol* 275: C1–C24, 1998. [PubMed: 9688830]
35. Lee MR, Li L, Kitazawa T. Cyclic GMP causes Ca^{2+} desensitization in vascular smooth muscle by activating the myosin light chain phosphatase. *J Biol Chem* 272: 5063–5068, 1997. [PubMed: 9030570]
36. Levine DZ, Iacovitti M, Burns KD, Zhang X. Real-time profiling of kidney tubular fluid nitric oxide concentrations in vivo. *Am J Physiol Renal Physiol* 281: F189–F194, 2001. [PubMed: 11399660]
37. Li L, Watts SW, Banes AK, Galligan JJ, Fink GK, Chen AF. NADPH oxidase-derived superoxide augments endothelin-1-induced venoconstriction in mineralocorticoid hypertension. *Hypertension* 42: 316–321, 2003. [PubMed: 12885792]
38. Loutzenhiser R, Bidani A, Chilton L. Renal myogenic response: kinetic attributes and physiologic role. *Circ Res* 90: 1316–1324, 2002. [PubMed: 12089070]
39. Luo CH, Rudy Y. A dynamic model of the cardiac ventricular action potential. I. Simulations of ionic currents and concentration changes. *Circ Res* 74: 1071–1096, 1994. [PubMed: 7514509]
40. Malinski T, Taha Z, Grunfeld S, Patton S, Kapturczak M, Tomboulis P. Diffusion of nitric oxide in the aorta wall monitored in situ by porphyrinic microsensors. *Biochem Biophys Res Commun* 193: 1076–1082, 1993. [PubMed: 8323533]
41. Mbikou P, Fajmut A, Brumen M, Roux E. Contribution of Rho kinase to the early phase of the calcium-contraction coupling in airway smooth muscle. *Exp Physiol* 96: 240–258, 2011. [PubMed: 20870731]
42. Meininger GA, Davis MJ. Cellular mechanisms involved in the vascular myogenic response. *Am J Physiol Heart Circ Physiol* 263: H647–H659, 1992. [PubMed: 1415587]
43. Nakanishi K, Mattson DL, Cowley SW Jr. Role of renal medullary blood flow in the development of l-NAME hypertension in rats. *Am J Physiol Regul Integr Comp Physiol* 268: R317–R323, 1995. [PubMed: 7864223]
44. Olson JL, Wilson SK, Heptinstall RH. Relation of glomerular injury to preglomerular resistance in experimental hypertension. *Kidney Int* 29: 849–857, 1986. [PubMed: 3712968]
45. Racasan S, Joles JA, Boer P, Koomans HA, Braam B. NO dependency of RBF and autoregulation in the spontaneously hypertensive rat. *Am J Physiol Renal Physiol* 285: F105–F112, 2003. [PubMed: 12631552]

46. Ren Y, D'Ambrosio MA, Liu R, Ragano PJ, Garvin JL. Enhanced myogenic response in the afferent arteriole of spontaneously hypertensive rats. *Am J Physiol Heart Circ Physiol* 298: H1769–H1775, 2010. [PMCID: PMC2886653] [PubMed: 20363886]
47. Schnackenberg CG, Welch WJ, Wilcox CS. Normalization of blood pressure and renal vascular resistance in SHR with a membrane-permeable superoxide dismutase mimetic. *Hypertension* 32: 59–64, 1998. [PubMed: 9674638]
48. Schnackenberg CG, Wilcox CS. Two-week administration of Tempol attenuates both hypertension and renal excretion of 8-Iso prostaglandin F₂. *Hypertension* 33: 424–428, 1999. [PubMed: 9931141]
49. Sgouralis I, Layton AT. Autoregulation and conduction of vasomotor responses in a mathematical model of the rat afferent arteriole. *Am J Physiol Renal Physiol* 303: F229–F239, 2012. [PMCID: PMC3404589] [PubMed: 22496414]
50. Sharma K, Cook A, Smith M, Valancius C, Inscho EW. TGF- β impairs renal autoregulation via generation of ROS. *Am J Physiol Renal Physiol* 288: F1069–F1077, 2005. [PubMed: 15644487]
51. Skov K, Mulvany MJ, Korsgaard N. Morphology of renal afferent arterioles in spontaneously hypertensive rats. *Hypertension* 20: 821–827, 1992. [PubMed: 1452298]
52. Smirnov SV, Loutzenhiser K, Loutzenhiser R. Voltage-activated Ca²⁺ channels in rat renal afferent and efferent myocytes: no evidence for the T-type Ca²⁺ current. *Cardiovasc Res* 97: 293–301, 2013. [PubMed: 23042470]
53. Stasch JP, Schmidt PM, Nedvetsky PI, Nedvetskaya TY, Meurer S, Deile M, Taye A, Knorr A, Lapp H, Müller H, Turgay Y, Rothkegel C, Tersteegen A, Kemp-Harper B, Müller-Esterl W, Schmidt HH. Targeting the heme-oxidized nitric oxide receptor for selective vasodilatation of diseased blood vessels. *J Clin Invest* 116: 2552–2561, 2006. [PMCID: PMC1555649] [PubMed: 16955146]
54. Toda N, Ayajiki K, Okamura T. Interaction of endothelial nitric oxide and angiotensin in the circulation. *Pharmacol Rev* 59: 55–75, 2007. [PubMed: 17329548]
55. Trottier G, Triggle CR, O'Neill SK, Loutzenhiser R. Cyclic GMP-dependent and cyclic GMP-independent actions of nitric oxide on the renal afferent arteriole. *Br J Pharmacol* 125: 563–569, 1998. [PMCID: PMC1565643] [PubMed: 9806341]
56. Ungvari Z, Csiszar A, Huang A, Kaminski PM, Wolin MS, Koller A. High pressure induces superoxide production in isolated arteries via protein kinase C-dependent activation of NAD(P)H oxidase. *Circulation* 108: 1253–1258, 2003. [PubMed: 12874194]
57. Vaziri ND. Roles of oxidative stress and antioxidant therapy in chronic kidney disease and hypertension. *Curr Opin Nephrol Hypertens* 13: 93–99, 2004. [PubMed: 15090865]
58. Wang X, Cupples WA. Interaction between nitric oxide and renal myogenic autoregulation in normotensive and hypertensive rats. *Can J Physiol Pharmacol* 79: 238–245, 2001. [PubMed: 11294600]

59. Wu R, Millette E, de Champlain J. Enhanced superoxide anion formation in vascular tissues from spontaneously hypertensive and desoxycorticosterone acetate-salt hypertensive rats. *J Hypertens* 19: 741–748, 2001. [PubMed: 11330877]
60. Yang J, Clark JW Jr, Bryan RM, Robertson C. The myogenic response in isolated rat cerebrovascular arteries: smooth muscle cell model. *Med Eng Phys* 25: 691–709, 2003. [PubMed: 12900184]
61. Yang J, Clark JW Jr, Bryan RM, Robertson C. Mathematical modeling of the nitric oxide/cGMP pathway in the vascular smooth muscle cell. *Am J Physiol Heart Circ Physiol* 289: H886–H897, 2005. [PubMed: 15833804]
62. Yoshida Y, Su HT, Cai JQ, Imai S. Cyclic GMP-dependent protein kinase stimulates the plasma membrane Ca^{2+} pump ATPase of vascular smooth muscle via phosphorylation of a 240-kDa protein. *J Biol Chem* 266: 19819–19825, 1991. [PubMed: 1655796]
63. Zahler R, Zhang ZT, Manor M, Boron WF. Sodium kinetics of Na,K-ATPase alpha isoforms in intact transfected HeLa cells. *J Gen Physiol* 110: 201–213, 1997. [PMCID: PMC2233788] [PubMed: 9236212]
64. Zalba G, Beaumont FJ, San José G, Fortuño A, Fortuño MA, Etayo JC, Díez J. Vascular NADH/NADPH oxidase is involved in enhanced superoxide production in spontaneously hypertensive rats. *Hypertension* 35: 1055–1061, 2000. [PubMed: 10818064]

Figures and Tables

Fig. 1.



[Open in a separate window](#)

Schematic diagram of the signaling pathways in an afferent arteriole smooth muscle cell. Not shown are background channels, inward- and delayed-rectifier K^+ channels, and buffering reactions. The contractile force depends on the fraction of myosin light chains (MLC) that are phosphorylated. The model represents the effects of nitric oxide (NO) and O_2^- on Ca^{2+} -activated K^+ (K_{Ca}) and L-type Ca^{2+} channels, plasma membrane (PMCA) and sarco/endoplasmic reticulum (SERCA) Ca^{2+} pumps, Na^+ - K^+ -ATPase, and myosin light chain phosphatase (MLCP) activation. MLCK, myosin light chain kinase; NCX, Na^+ / Ca^{2+} exchanger. See text for meaning of other symbols.

Table 1.

Smooth muscle cell mechanical parameters

Parameter	Value	Unit
C_{pass}	1,693.07	dyn/cm
C'_{pass}	6.0	Dimensionless
C''_{pass}	-2,250.0	dyn/cm
C_{act}	15,287.7	dyn/cm
C'_{act}	1.0	Dimensionless
C''_{act}	0.472965	Dimensionless
D_0	24.0	μm
τ_d	2.0	s

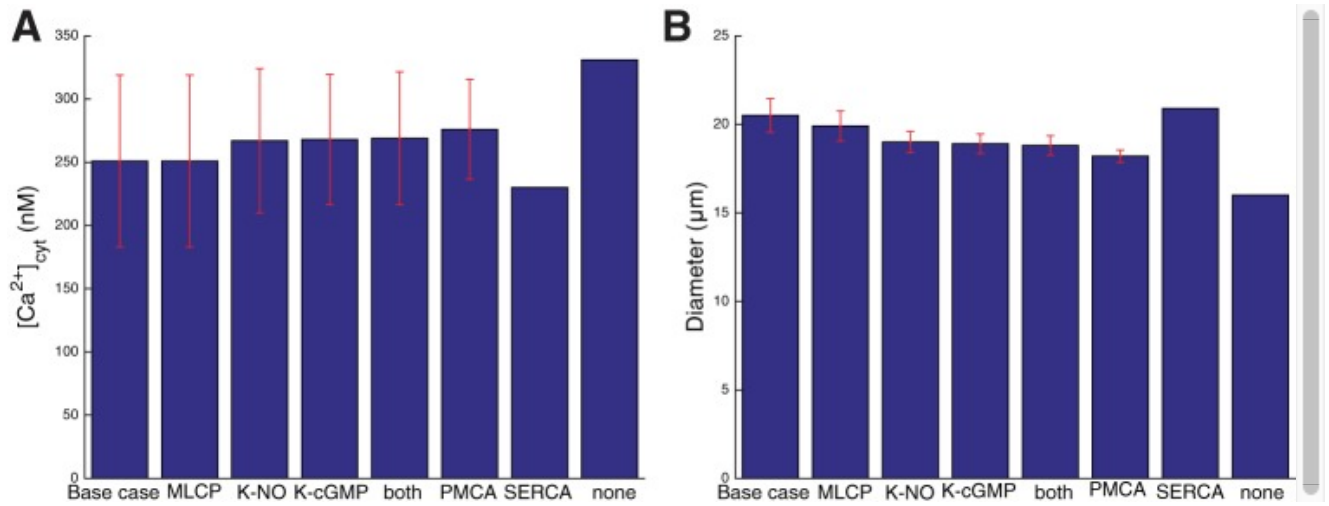
[Open in a separate window](#)**Table 2.**

Assumed differences between rat strains

Parameter	SD	SHR
$G_{\text{O}_2^-}$, $\mu\text{M/s}$	14.4	36.0
k_1^{sGC} , $\mu\text{M/s}$	2×10^3	2×10^2
γ_{RK} , $\mu\text{M/s}$	0.30	0.45

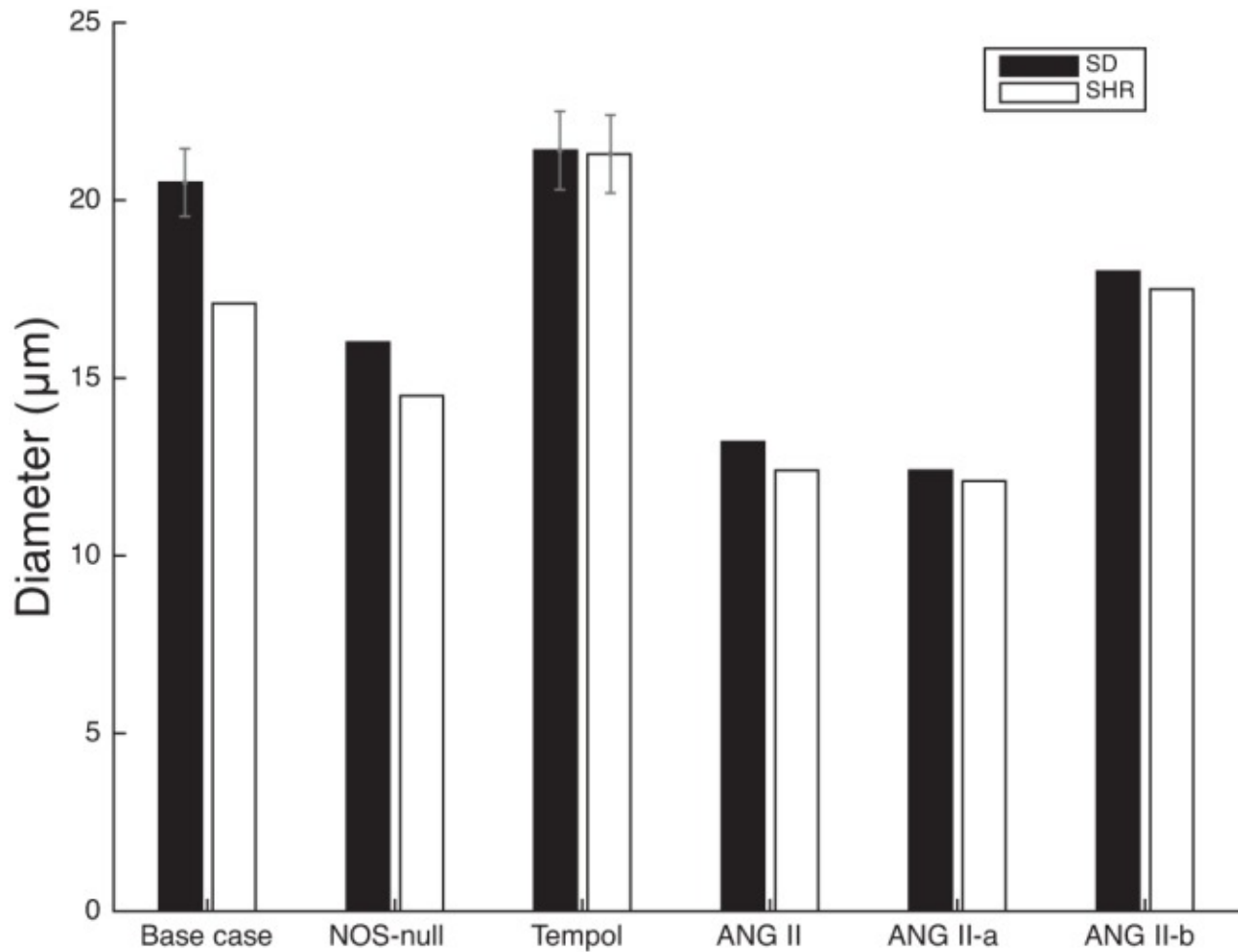
$G_{\text{O}_2^-}$, O_2^- production rate at 100 mmHg; k_1^{sGC} , forward rate constant of the reaction between nitric oxide and basal soluble guanylate cyclase ([Eq. 11](#)); γ_{RK} , Ca^{2+} dependence of RhoK activation ([Eq. 43](#)); SD, Sprague-Dawley rats; SHR, spontaneously hypertensive rats.

Fig. 2.



Contributions of individual vasodilatory pathways in the afferent arteriole of Sprague-Dawley (SD) rats, assuming a luminal pressure of 100 mmHg. Red bars indicate the range of cytosolic Ca²⁺ concentration (A) and vessel diameter (B) in spontaneous vasomotion. MLCP, without cGMP modulation of MLC phosphatase activity; K-NO, without NO modulation of K_{Ca} current; K-cGMP, without cGMP modulation of K_{Ca} current; both, without NO and cGMP modulation of K_{Ca} current; PMCA, without cGMP modulation of PMCA activity; SERCA, without cGMP modulation of SERCA activity; none, in the absence of NO and cGMP.

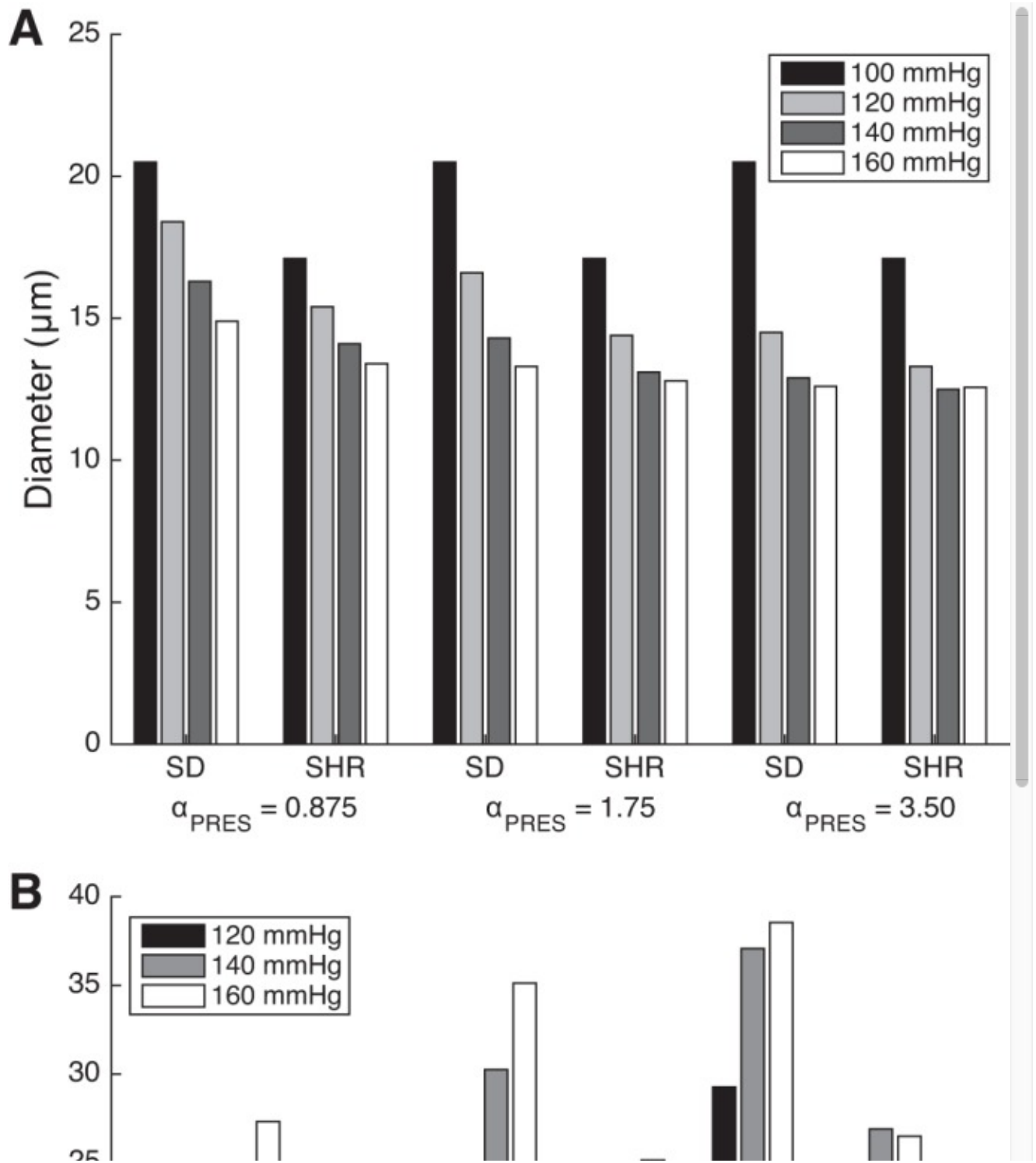
Fig. 3.



[Open in a separate window](#)

Effects of NO, O_2^- , and angiotensin (ANG) II on the afferent arteriole diameter of SD and spontaneously hypertensive rats (SHR), under different conditions: NOS-null, full nitric oxide synthase (NOS) inhibition; Tempol, 100 μ m; ANG II, addition of ANG II simulated with a 2-fold increase in IP_3 and O_2^- production, and 60% inhibition of K^+ channels; ANG II-a, ANG II and full NOS inhibition; ANG II-b, ANG II with NO donor (900 nM NO). Red bars indicate the diameter range in spontaneous vasomotion.

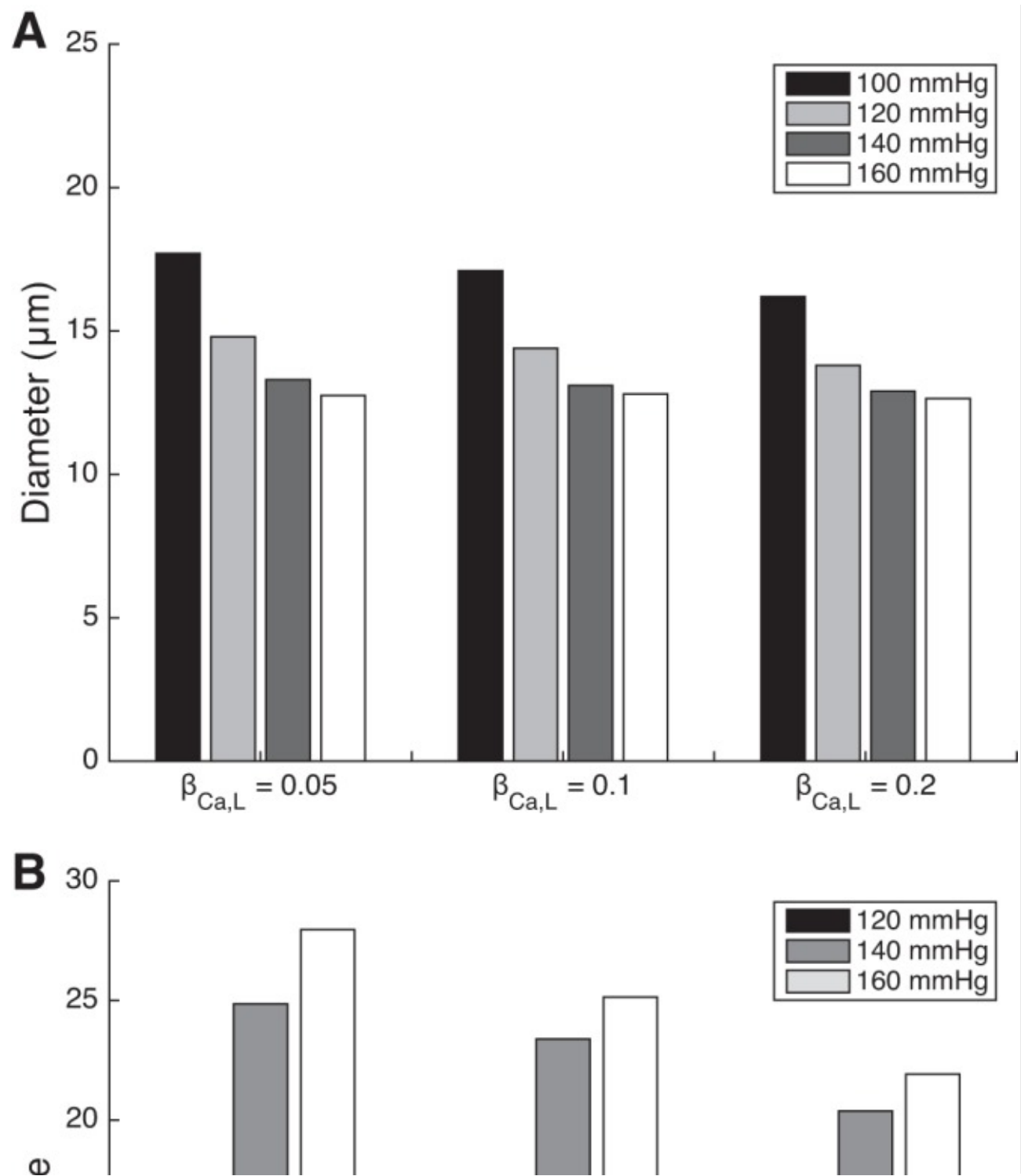
Fig. 4.



[Open in a separate window](#)

Predicted effects of varying the pressure-dependence of mechanosensitive channels (α_{PRES}) on the myogenic response of SD and SHR rats. *A*: afferent arteriolar diameter at a luminal pressure of 100, 120, 140, and 160 mmHg, for 3 values of α_{PRES} (baseline $\alpha_{PRES} = 1.75$). *B*: fractional change in diameter, relative to that at 100 mmHg.

Fig. 5.

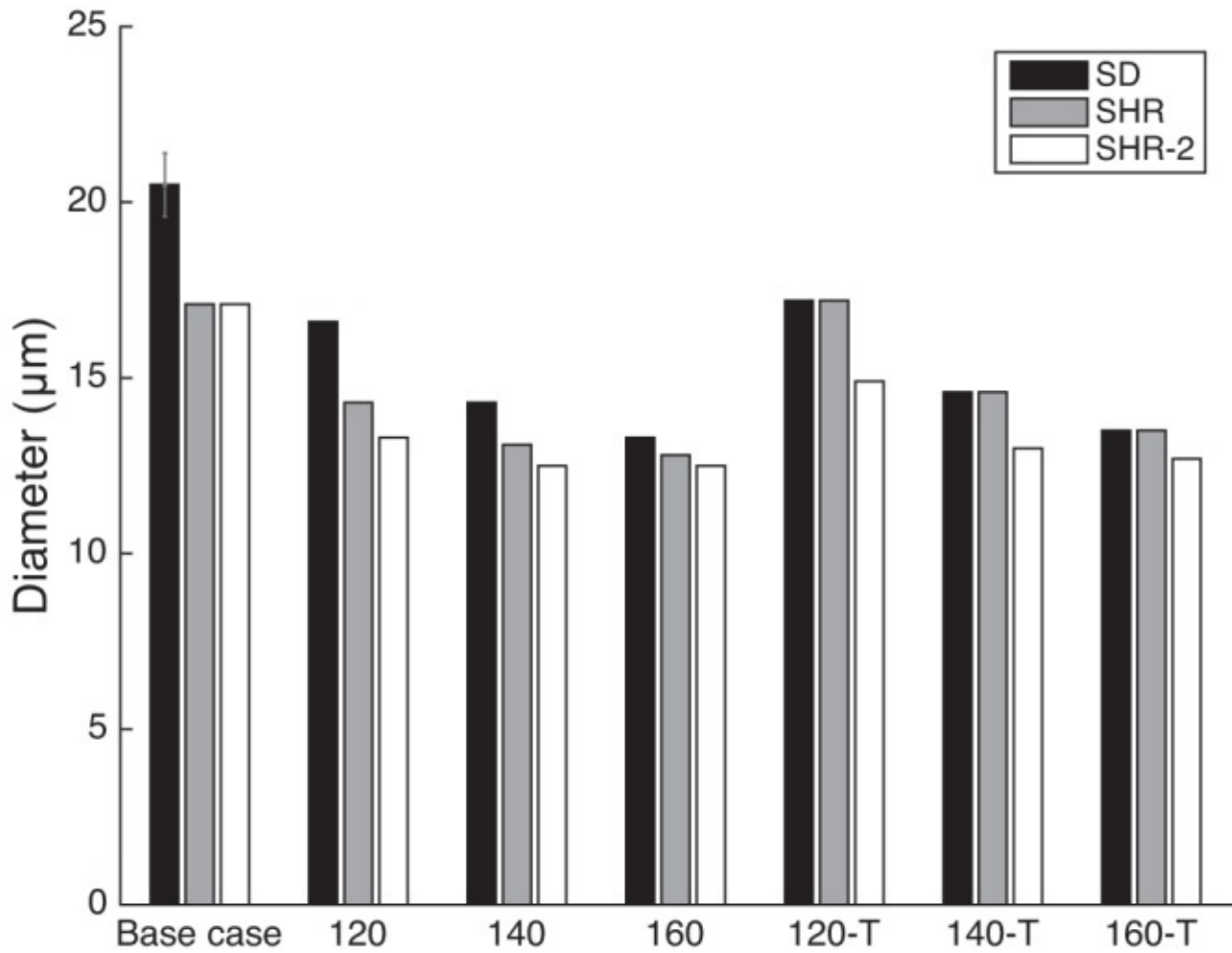


[Open in a separate window](#)

Predicted effects of varying the $[O_2^-]_{cyt}$ dependence of the L-type channel conductance ($\beta_{Ca,L}$) on the myogenic response of SHR. *A*: afferent arteriolar diameter at a luminal pressure of 100, 120, 140, and 160 mmHg, for 3 values of $\beta_{Ca,L}$ (baseline $\beta_{Ca,L} = 0.10$). *B*: fractional change in diameter, relative to that at 100 mmHg. The myogenic response in

normotensive rats is insensitive to changes in $\beta_{Ca,L}$.

Fig. 6.



[Open in a separate window](#)

Effects of perfusion pressure and Tempol on the afferent arteriole diameter of SD and SHR. Case labels indicate perfusion pressure in mmHg. Perfusion pressure equals 100 mmHg in the base case. “-T” denotes the addition of 100 μ M Tempol. The value of α_{PRES} is set to 1.75 in SD, and 1.75 and 3.5 in SHR (denoted “SHR” and “SHR-2,” respectively). As observed experimentally, Tempol affects the myogenic response in SHR but not in normotensive rats.

Table 3.

Key model predictions for normotensive and spontaneously hypertensive rats

	SD			SHR		
	Base case	140 mmHg	NOS inhibition	Base case	140 mmHg	NOS inhibition
AA diameter, μm	20.5 (1.9)	14.3	16.0	17.1	13.1	14.5
$[\text{NO}]_{\text{cyt}}$, nM	152	147	0	100	76	0
$[\text{O}_2^-]_{\text{cyt}}$, nM	4.9	5.6	7.6	14.0	22.1	18.9
$[\text{cGMP}]$, μM	11.1	11.0	0.027	5.3	4.5	0.027
$G_{\text{O}_2^-}$, $\mu\text{M}\cdot\text{s}^{-1}$	14.4	16.1	14.4	36.0	53.3	36.0
k_2^{Myo} , s^{-1}	0.150	0.108	0.118	0.113	0.085	0.096
$G_{\text{Ca,L}}$, nS	2.75	2.78	2.89	3.24	3.69	3.51
$G_{\text{Ca,Pres}}^0$, nS	0.0200	0.0527	0.0200	0.0200	0.0527	0.0200
V_{KCa} , mV	88.7 (10.8)	75.5	192.9	97.0	84.5	189.7
$I_{\text{PMCA,max}}$, pA	4.96	4.96	4.55	4.92	4.91	4.55
K_{mf} , nM	307	307	574	320	324	574

Numbers in parenthesis indicate amplitude when oscillations are present.

AA, afferent arteriole; NOS, nitric oxide synthase.

See MATHEMATICAL MODEL for the meaning of other parameters.

Articles from American Journal of Physiology - Renal Physiology are provided here courtesy of **American Physiological Society**